BUTTERWORTH HEINEMANN

Polymer Vol. 36 No. 25, pp. 4741–4752, 1995

0032-3861/95/$10.00 + 0.00

Stress-induced shifts and intensity changes in the 1616 cm^{-1} Raman line for isotropic and uniaxially oriented poly(ethylene terephthalate)

E. L. V. Lewis, D. I. Bower* and I. M. Ward
Department of Physics, The University of Leeds, Leeds LS2 9JT, UK
(Received 10 November 1994; revised 20 March 1995)

Measurements of the shifts induced in the 1616 cm^{-1} Raman line by applied stress have been made for an isotropic undrawn sample and several uniaxially oriented samples of poly(ethylene terephthalate) using various polarization directions of incident and scattered light with respect to the sample and to the direction of the stress, which was applied either parallel or perpendicular to the draw direction for the uniaxial samples. The corresponding changes in intensity with applied stress were also determined. The experiments and analysis are described in detail. The observed shifts for different conditions have previously been shown to be in accord with interrelationships predicted by a formal theoretical treatment, but no physical interpretation was attempted. This is now done, but it is not found possible to interpret the shifts satisfactorily in terms of a simple physical model. A model in which the average shift contributed by chains at a specific angle to the draw direction is assumed to be determined by the macroscopic short-time strain resolved with respect to the chain axes fits the data slightly better than one where the macroscopic stress plays the corresponding role, though neither model fits the data well. In spite of this, the observed shifts depend only on the applied stress and do not change as the sample creeps. The changes of intensity observed with applied stress could not be explained fully in terms of changes of molecular orientation, and it is concluded that the application of stress also changes the magnitude and form of the Raman tensor.

(Keywords: poly(ethylene terephthalate); Raman; line shifts)

INTRODUCTION

We have recently presented some very general considerations concerning the shifts observed in the Raman spectra of random and uniaxially oriented polymers when they are subjected to a uniaxial stress[1]. It was shown that certain relationships should exist between the shifts observed with different polarization conditions. Experimental data on the 1616 cm^{-1} line of poly(ethylene terephthalate) (PET) were found to be consistent with the predictions. The experimental details involved in obtaining the data were not described, nor was any attempt made to interpret the data beyond comparison with the formal relationships. It is the purpose of the present paper to explain in detail how the data were obtained and to discuss the observed shifts in terms of various models which relate them to either the macroscopic stress or the macroscopic strain of the sample. The observed changes of intensity on loading will also be discussed, but discussion of the changes in linewidth and line shape that were also observed to accompany the shifts will be deferred to a subsequent paper.

The present work represents a continuation of that reported earlier[2], in which it was shown that measurements of Raman shifts could be made on moderately, rather than highly, oriented PET and that it might prove possible to obtain information about the distribution of stresses on molecules at different orientations to the draw direction, provided that observations were made with different polarization combinations. This work was in turn suggested by the considerable number of papers that had appeared in recent years reporting the effect of applied stresses on the infra-red and Raman spectra of oriented polymers[1]. Almost all of those studies were, however, concerned with highly or very highly oriented polymers, and generally neither the effect of the polarization of the incident and scattered light on the shift observed in Raman studies nor the effect of the direction of the applied stress was considered.

EXPERIMENTAL

Materials and preparation

For most of the work the starting material was amorphous poly(ethylene terephthalate) (ICI) in the form of undrawn sheet 188 ± 5 μm thick. It was optically isotropic and clear, and had a refractive index of 1.5750 and a density of 1.3385 $Mg\,m^{-3}$.

Dumb-bells of length 110 mm and width 60 mm, with a narrower central region 35 mm long and 40 mm wide,

* To whom correspondence should be addressed

were cut from this sheet and drawn at $81 \pm 1°C$ and $5\,mm\,min^{-1}$ without necking to a selection of different final draw ratios (λ) up to the maximum obtainable, in an Instron tensile tester (model 1026, oven 3111); they were then allowed to cool at constant length to room temperature, and were subsequently aged in an air oven (RDP-Howden), together with an undrawn sheet, all hanging freely with small weights to keep them straight, for five days at $60 \pm 1°C$ to stabilize their properties. The sheets subsequently used were called A (undrawn), B (draw ratio 3.38) and C (draw ratio 4.71).

An additional PET sample, called D, was prepared from a sheet of ICI Melinex film (intrinsic viscosity ~ 0.74, thickness 240 μm), which was drawn at 80°C and $\sim 10\,mm\,min^{-1}$ to a draw ratio of 3.93 in a T. M. Long film stretcher, then heat set by annealing at constant load at 140°C for 5 min. The final thickness was 125 μm. This sheet was not aged.

There were slight variations in the draw ratio at different parts of each sample and the values quoted should be considered accurate to $\sim \pm 0.03$.

Characterization of drawn samples

The thicknesses of the sheets A–C ranged from 188 μm for the undrawn sheet to 82 μm for the highest draw ratio (4.71); the density range was from 1.3385 to $1.3623 \pm 0.0002\,Mg\,m^{-3}$, giving a crystallinity from 0 to 23% by volume[3]. Sheet D had a higher crystallinity and degree of orientation, as determined from wide-angle X-ray diffraction photographs. The axes used in reporting the properties are defined as follows[4]: OX_3 is parallel to the draw direction, OX_2 is normal to the sheet and OX_1 is the transverse direction.

The refractive indices of samples from the sheets A–D were measured in sodium D light (589.3 nm) using an Abbe refractometer (Bellingham & Stanley, model 60/ED), and the results are in *Table 1*. The samples were optically uniaxial within experimental uncertainties. The fractional reductions in the width and thickness of the samples due to drawing were found to be the same, confirming the uniaxial nature of the drawing. Additional measurements of refractive index and birefringence were made on a Zeiss Interphako interference microscope and on a Zeiss Polmi A polarizing microscope fitted with an Ehringhaus compensator, as these methods more closely resembled the transmission method of the Raman measurements themselves.

Further confirmation of the uniaxial nature of the samples came from wide-angle X-ray diffraction (WAXD) studies using a Siemens two-circle diffractometer and a Huber four-circle texture goniometer. The Siemens diffractometer was used to look at the equatorial reflections 010, $1\bar{1}0$ and 100 for orientation of the *a* and *b* axes and hence of the planes of the chains around the draw direction; the Huber goniometer was used to study the (almost) meridional reflection $\bar{1}05$ for any indication of orientation of the chain *c* axes themselves around the draw direction. Neither method showed any preferred orientation around the draw direction.

Tapes 1 mm wide by 50 mm long were cut from the aged sheets parallel to draw and 1 mm by the width of the drawn sheet perpendicular to draw for mechanical and Raman measurements.

Mechanical measurements

The behaviour of the drawn samples under tensile load at room temperature was found for each draw ratio using a self-aligning modification of an extensional creep apparatus[5] with a calibrated transducer (Penny & Giles, model L.V.D.T. D.S. 1303) mounted on a rod below the lower grip. Cycles of conditioning at the

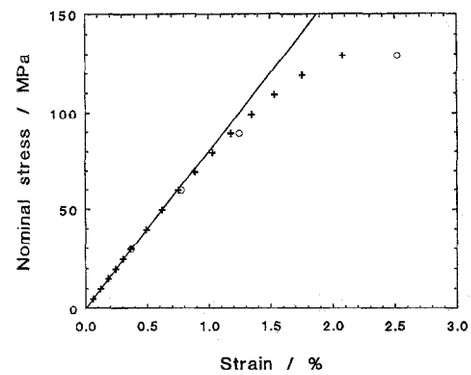

Figure 1 Stress–strain curves for sample C ($\lambda = 4.71$) loaded parallel to the draw direction: (+) 10 s loading, where the points in the linear region up to 0.6% strain were used for the straight line fit shown; (○) 700 s loading

Table 1 Refractive indices of samples of sheets

Sample sheet	Draw ratio λ	Method[a]	Refractive indices			Birefringence[b]
			n_3	n_2	n_1	
A	1	Ab	1.5752	1.5746	1.5752	0.0003 (2)
B	3.38	Ab	1.6203	1.5620	1.5630	0.0580 (4)
		In	1.6230		1.5623	0.060 (1)
		Co				0.062 (1)
C	4.71	Ab	1.6630	1.5478	1.5473	0.1154 (4)
		In	1.674		1.548	0.126 (2)
		Co				0.129 (1)
D	3.93	Ab	1.6961	1.5440	1.5469	0.151 (1)
		In	1.6935		1.5474	0.146 (2)
		Co				0.181 (2)

[a] Ab, Abbe refractometer; In, Interphako microscope; Co, Ehringhaus compensator
[b] Figures in parentheses are uncertainties in the preceding figure

highest stresses to be used ensured reproducibility[6–8], and also removed a non-recoverable displacement upon initial loading, which was equivalent to a strain between 0.013 and 0.040%. Displacements were noted 10 s after applying each load; *Figure 1* shows the stress–strain curves for sample C for loading parallel to draw.

The 10 s extensional compliances s_{33} (parallel to draw) and s_{11} (perpendicular to draw) were found from the gradients of the initial linear regions of the stress–strain curves and the results are given in *Table 2*. Corrections were made for apparatus displacement with load and, where possible, for end or grip effects[9].

The creep behaviour, and hence the creep compliance at longer times, was found by taking readings of the displacement at various intervals up to 20 min after loading for four loads covering the range of stresses used in the 10 s measurements. Hence the strain for any given stress and time during the Raman studies could be found by interpolation. *Figure 1* also shows the strains 700 s after loading sample C parallel to draw.

Two non-reversible effects were discovered in these studies. The first was that samples from sheet B of draw ratio 3.38 necked when taken above their yield stress parallel to draw of 80 MPa. In the Raman measurements the stress was kept below the yield stress. The second was a fine crazing, with craze lines normal to the stress direction: this occurred in samples from the undrawn sheet A, and in samples from sheets B and C when stressed perpendicular to the draw direction. This was avoided in the Raman studies by keeping the stress below the crazing level.

Raman spectroscopy

The Raman stress studies were done on samples from sheets of three draw ratios (B, C and D), as well as on the undrawn sheet A. Samples were mounted in a device designed to allow the sample to be rotated to any angle about a vertical (stress) axis and also adjusted accurately to any height with respect to the light beam, so that exactly the same region could be brought back into the beam after loading (see the Appendix). Samples were illuminated by the linearly polarized beam from a Spectra-Physics 2016-05 argon ion laser tuned to 488.0 nm, with TEM_{00} output in the light-stabilized mode. The beam was horizontal and passed through a prism monochromator to eliminate the argon plasma lines and then through a half-wave plate, which permitted the electric vector of the incident beam to be set vertical (V) or horizontal (H). Both 90° and 180° (back-scattering) scatter geometries (SGs) were used in the study; these are called X_iX_j, where OX_i and OX_j are the directions of the incident ray and scattered ray, respectively, with respect to the sample; 180° SGs are X_iX_i/k, where k is the direction of applied stress (vertical) with respect to the axes $OX_1X_2X_3$. In the 90° SGs, whenever the beam was incident on the large face, the sample was positioned so that the distance the scattered ray travelled through the sample was minimal, so as to minimize any effects of polarization scrambling (see the Appendix). The Raman intensities are denoted by I_{ij}, where i stands for the direction of the electric vector of the scattered beam and j for that of the incident beam.

The scattered light was focused onto the entrance slit of a Coderg PHo double monochromator through an analyser (vertical (v) or horizontal (h)) and then a quarter-wave plate, which acted as a polarization scrambler. The best width setting of the spectrometer slits was found to correspond to 2 cm^{-1} (maximum intensity with negligible line distortion). The scattered light was detected by an EMI S-20 photomultiplier, cooled to −30°C by a Peltier cooler, and the signal processed by suitable electronics including digitization and co-adding of several sweeps of each spectrum so as to improve the signal-to-noise ratio. The laser power incident on the sample was simultaneously monitored by means of a beam splitter, and stored during each run. When the beam was incident on the large face of the sample, the laser power output was 1.0 W and the power on the sample was ~ 360 mW, partially focused by a lens of focal length +150 mm into a disc of ~ 0.6 mm diameter. Whenever the beam was incident on the sample edges, it was focused exactly, and the power was reduced to a third of the above value. The digitized results were analysed on an Amdahl 5860 mainframe computer, with software specially written for the purpose.

To check for the presence of any filler in the samples, full Raman spectra from 300 to 1836 cm^{-1} were run for two undrawn samples, the second being from a PET sheet E known to have no filler. The spectra, scaled to the same peak intensity at the 1616 cm^{-1} line, were subtracted; the difference showed no sharp extra lines[10]. WAXD showed no extra peaks, either.

Before any sample was loaded, 'never-loaded' spectra were obtained, co-adding ~ 20 sweeps for each polarization combination, to determine the line shape more precisely, so that the effects of initial loading and unloading could be studied.

Preliminary experiments showed that the peak position of the 1616 cm^{-1} line remained constant from immediately after loading and during individual sweeps up to at least 12 min after loading (the length of each subsequent run). Each sample was conditioned by applying the load for 10 s and then removing it for ~ 2 min to allow the sample to relax; this was repeated

Table 2 Measured 10 s compliances

Sample sheet	Draw ratio λ	s_{33} (GPa^{-1})	l_g[a] (mm)	s_{11} (GPa^{-1})	l_g[a] (mm)
A	1	0.439 ± 0.004	39.1	(0.439 ± 0.004)[b]	(39.1)[b]
B	3.38	0.240 ± 0.003	39.9	0.462 ± 0.010	inf.
C	4.71	0.116 ± 0.002	inf.	0.481 ± 0.032	inf.
D	3.93	0.105 ± 0.002	40.0	0.532 ± 0.005	26.3

[a] Length between the grips; 'inf.' means corrected to infinite length, so that end or grip effects are removed
[b] For an isotropic sample s_{11} and s_{33} are equivalent

twice. Load cycling was then performed as follows. A conditioned unloaded run was done first, the load was then applied, and scanning was started 3 min afterwards; for each run, three sweeps were co-added, taking 9 min (12 min after loading); the load was then removed, and the sample allowed to relax for at least 45 min before the cycle of unloaded and loaded spectra was repeated. This procedure was carried out three to six times in order to ensure reproducibility and increase precision for each polarization combination, SG and load. The spectral range recorded was 1537–1665 cm^{-1} at 0.25 cm^{-1} intervals at a speed of 50 cm^{-1} min^{-1}.

The wavenumber calibration of the spectrometer was monitored before and after each run using a line of a neon lamp at 1733 cm^{-1}; changes in calibration could be corrected to within ~ 0.01 cm^{-1}. The degree of depolarization of the beam transmitted through each sample was also measured; the results are shown in *Table A1* of the Appendix, which also gives the absorption or scattering (and reflection) of the transmitted beam.

DATA ANALYSIS

Although the 1616 cm^{-1} line is slightly asymmetric, a Lorentzian curve with horizontal linear background was fitted to each spectrum in the first analyses, and the centre of this curve taken as the position of the line. The curves were fitted over the full recorded range (1537–1665 cm^{-1}) and also a limited range of 1600–1630 cm^{-1} for the line region only: these fits were found to give similar line positions, so that only the full range was subsequently used. Later, a split Lorentzian was fitted over the full range: in this fit the two half-widths, at wavenumbers below and above the position of maximum intensity, were fitted independently, with an overall single sloping linear background. The position of maximum intensity (peak) was one of the fitted parameters, and this was taken as the position of the line. Each spectrum for unloaded and loaded samples was analysed individually, and the corresponding results averaged. This was carried out for both Lorentzian and split Lorentzian fits. These two methods of finding the line shifts did not differ significantly, so the weighted mean of the shifts calculated by the two methods was taken to be the best measure of each shift.

The shift in peak position may not be the most appropriate measure when comparing shifts with theoretical predictions, where the shift in the centre of gravity might be more appropriate. It is, however, very difficult to determine the centre of gravity of the line experimentally because its apparent position can be strongly affected by the choice of baseline and truncation limits if raw data are used, or by these and the choice of line shape if fitted peaks are used.

RESULTS

Refractive indices

The refractive indices in *Table 1* show the expected variation with draw ratio for samples A, B and C, but the different methods of measuring them yield slightly different values and hence different birefringences, a phenomenon found also by Bower *et al.*[11]. It was concluded there that transmission methods (Interphako and compensator) were more appropriate to the Raman studies, so that the weighted means from those methods have been used here in deriving orientation averages for comparison with the Raman results.

Raman intensity ratios and molecular orientation

The Raman intensities were corrected for the total laser power incident, differences in the intensities of the incident beam when vertically (V) or horizontally (H) polarized, the different sensitivities of the spectrometer to scattered radiation polarized vertically (v) or horizontally (h), and refractive index effects such as the variation of light transmission through surfaces and the different volumes of the cones of light accepted by the spectrometer lens and slit[12]. Sets of intensities from different SGs were then co-scaled subject to the constraint that $I_{33} = 100$, in the way described by Jarvis *et al.*[4]

The resulting intensities for the drawn sheet C did not

Table 3 Raman intensities for different polarization combinations and samples

	Samples			
Intensity	A[a] ($\lambda = 1$)	B[b] ($\lambda = 3.38$)	C[b] ($\lambda = 4.71$)	D[c] ($\lambda = 3.93$)
I_{11}	100.2	27.9 ± 0.6	10.0 ± 1.5	10.7 ± 0.5
I_{22}	102.9	28.6	10.5 ± 0.9	9.4
I_{33}	100.0 ± 4.6	100.0 ± 0.3	100.0 ± 0.7	100.0 ± 0.1
I_{12}	67.5	18.7	9.8 ± 1.9	4.6
I_{21}	67.4	20.9 ± 0.2	9.5 ± 1.0	5.7
I_{13}	54.3 ± 7.5	19.2 ± 3.2	13.3 ± 0.8	10.1 ± 0.3
I_{31}	54.0 ± 6.6	22.4	15.7 ± 0.4	12.4 ± 0.7
I_{23}	86.8 ± 8.1	26.6 ± 0.2	17.8 ± 2.7	11.4 ± 1.0
I_{32}	94.4 ± 2.1		19.1 ± 4.3	12.2 ± 1.1
P_{200}^{c}	0	0.341 ± 0.004	0.611 ± 0.010	0.681 ± 0.010
P_{400}^{c}	0	0.233 ± 0.058	0.418 ± 0.035	0.702 ± 0.023
P_{2}^{opt}	0	0.265 ± 0.003	0.559 ± 0.005	0.763 ± 0.052

[a] Before correction for polarization scrambling
[b] After correction for differential scattering
[c] No corrections required for scattering or scrambling

show the expected relationships for a uniaxial sample, since I_{22} was greater than I_{11}, and I_{23} and I_{32} were greater than I_{13} and I_{31}. When the intensities for the undrawn sheet A were measured, it was found that $I_{22} \approx I_{11}$, but (I_{23} and I_{32}) > (I_{12} and I_{21}) > (I_{13} and I_{31}) (*Table 3*), whereas these last six intensities should all be equal. These discrepancies were eventually traced to the effects of polarization scrambling and differential scattering discussed in the Appendix, where a method of correcting for them is described.

The values of the intensities after correction are given for samples B, C and D in *Table 3*, which also shows the orientation averages $P^c_{200} = \langle P_2(\cos\theta)\rangle$ and $P^c_{400} = \langle P_4(\cos\theta)\rangle$ calculated from them, together with the value of $P_2^{opt} = \langle P_2(\cos\theta)\rangle$ calculated from the birefringences, assuming that P_2^{opt} is directly proportional to the birefringence and that the maximum birefringence[13] is 0.230. $\langle P_l(\cos\theta)\rangle$ is the mean value of the lth-order Legendre polynomial in θ, the angle between a typical chain axis and OX_3.

The orientation averages P^c_{200} and P^c_{400} were calculated from the theory of Jarvis *et al.*[4] for their model A, assuming that $P^c_{lmn} = 0$ for $m,n \neq 0$. A cylindrical Raman tensor with $r = \alpha_1/\alpha_3 = \alpha_2/\alpha_3 = -0.122 \pm 0.004$, derived from the measured linear depolarization ratio of 0.479 ± 0.005 of the undrawn sheet in SG X_2X_2, was used throughout. This value of r is lower than values used previously[4,11–13]; the justification for using it here is that it was measured on the undrawn material from which most of the present samples were made, and that it corresponds to a lower depolarization ratio than previously determined. The undrawn material had been carefully examined for evidence of orientation, and none was found. Any polarization scrambling could only raise the observed depolarization ratio. Huijts and Peters[14] have also recently obtained the value $r = -0.122 \pm 0.004$ for the 1616 cm^{-1} line.

The values of P^c_{200} for samples B and C are slightly greater than the corresponding values of P_2^{opt}, whereas the reverse is true for sample D. The reason for this is not understood, nor is the reason why P^c_{400} is greater than P^c_{200} for sample D, whereas the reverse is true for samples B and C, as expected. It is clear that there must be additional sources of error which are not accounted for in the uncertainties shown, which are based on scatter in repeated measurements.

Stress Raman effects

In the light of the findings in the Appendix, it was possible to select SGs and polarizations which avoided, as far as possible, the risk of any mixing in of other intensities via polarization scrambling or differential scattering. Early runs on samples from sheet C were done at four different loads, and it was found that the shift in line position was linear with stress at high stresses, and not so with strain (*Figure 2*). Subsequent runs were done with only one load, the maximum value.

The shifts, calculated as explained above, are shown in *Table 4*, expressed as stress sensitivities and as strain sensitivities. The stress sensitivities are plotted against the Raman orientation average P^c_{200} in *Figures 3* and *4*. The observed changes in intensity with stress are given in *Table 5*, together with the true applied stresses and the average strains during the time of collection of the Raman data, allowing for creep.

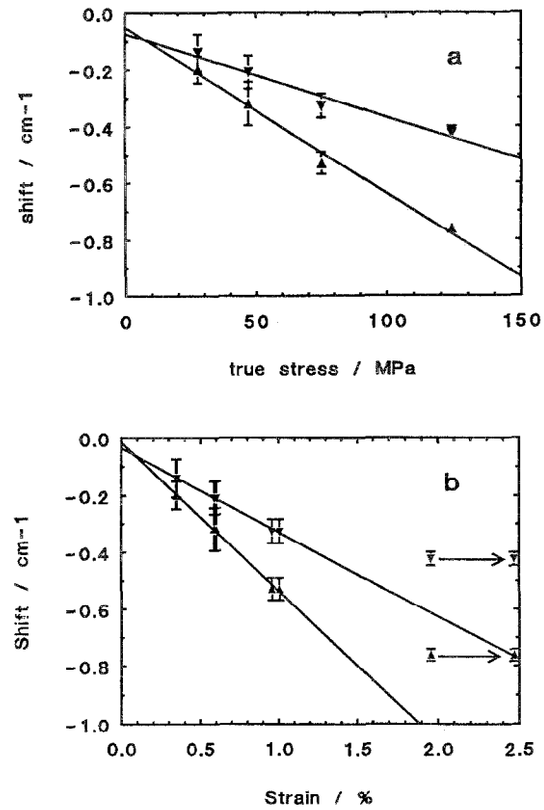

Figure 2 Shift of the 1616 cm^{-1} Raman line for sample C ($\lambda = 4.71$) against stress and strain for tensile loading parallel to the draw direction: (▲) Vv polarization (S_{33}); (▼) Vh polarization (S_{13}). (a) Shift plotted against nominal stress. (b) Shift plotted against strain, where the points linked by arrows represent the strains at 10 s and 700 s for the non-linear, time dependent region of strain

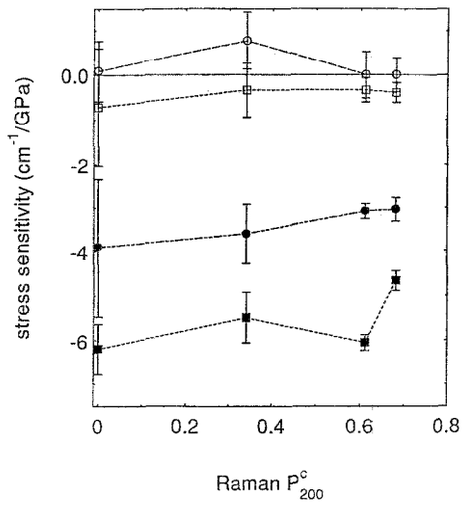

Figure 3 Stress sensitivity of the shift for the 1616 cm^{-1} Raman line for all samples, plotted against P^c_{200} for uniaxial stress parallel to the draw direction (OX_3): (○) s_{11}; (●) s_{13}; (□) s_{21}; (■) s_{33}

There was no change in line shape for the undrawn sample A with intensity I_{ij} (SG and polarization), suggesting that the line is single, as in crystals of bis(2-hydroxyethyl)terephthalate (BHET)[12,15]. The line shape was asymmetric even when the sample had never been loaded or was undrawn or both, and even in the undrawn sample E without filler. The corresponding line was

Table 4 Stress sensitivities and strain sensitivities of shifts

	Samples							
	A ($\lambda = 1$)		B ($\lambda = 3.38$)		C ($\lambda = 4.71$)		D ($\lambda = 3.93$)	
Shift	Value	Uncertainty[a]	Value	Uncertainty[a]	Value	Uncertainty[a]	Value	Uncertainty[a]
				Stress sensitivities (cm^{-1} GPa^{-1})				
Stress parallel to draw (OX_3)								
S^3_{33}	−6.19	0.56	−5.49	0.57	−6.05	0.18	−4.66	0.22
S^3_{11}	+0.08	0.68	+0.77	0.65	+0.00	0.52	−0.10	0.38
S^3_{21}	−0.72	1.31	−0.35	0.60	−0.34	0.27	−0.40	0.22
S^3_{13}	−3.90	1.57	−3.60	0.68	−3.08	0.17	−3.04	0.27
Stress perpendicular to draw (OX_1)[b]								
S^1_{33}	(+0.08)	(0.68)	+2.95	1.05	+4.64	0.55		
S^1_{11}	(−6.19)	(0.56)	−7.19	1.54	−10.11	1.54		
S^1_{22}	(+0.08)	(0.68)	−2.06	1.90	−4.04	2.27		
S^1_{21}	(−3.90)	(1.57)	−4.57	1.19	−5.05	1.60		
S^1_{13}	(−3.90)	(1.57)	−1.05	2.60	+5.06	1.26		
S^1_{23}	(−0.72)	(1.31)	−0.21	1.19	−0.61	1.08		
				Strain sensitivities (cm^{-1} $\%^{-1}$)				
Stress parallel to draw (OX_3)								
S^3_{33}	−0.135	0.012	−0.186	0.013	−0.395	0.011	−0.310	0.014
S^3_{11}	+0.002	0.015	+0.026	0.022	+0.000	0.024	−0.007	0.025
S^3_{21}	−0.016	0.029	−0.012	0.020	−0.021	0.016	−0.026	0.015
S^3_{13}	−0.085	0.034	−0.122	0.023	−0.187	0.010	−0.203	0.018
Stress perpendicular to draw (OX_1)[b]								
S^1_{33}	(+0.002)	(0.015)	+0.059	0.021	+0.082	0.010		
S^1_{11}	(−0.135)	(0.012)	−0.143	0.031	−0.180	0.027		
S^1_{22}	(+0.002)	(0.015)	−0.041	0.038	−0.071	0.040		
S^1_{21}	(−0.085)	(0.034)	−0.091	0.024	−0.089	0.028		
S^1_{13}	(−0.085)	(0.034)	−0.021	0.052	+0.090	0.022		
S^1_{23}	(−0.016)	(0.029)	−0.004	0.024	−0.011	0.019		

[a] Standard error of the mean

[b] The set of values for the isotropic sample A for 'Stress perpendicular to draw' is simply obtained from the set for 'Stress parallel to draw' by changing axes, since the 'draw' direction is arbitrary for an isotropic, undrawn sample

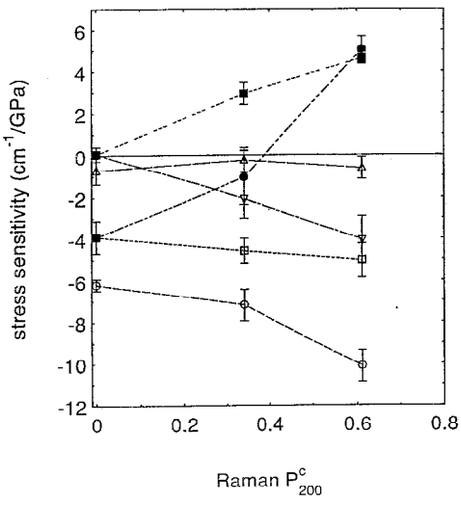

Figure 4 Stress sensitivity of the shift for the 1616 cm^{-1} Raman line for all samples, plotted against P^c_{200} for uniaxial stress perpendicular to the draw direction (OX_3): (○) s_{11}; (●) s_{13}; (□) s_{21}; (■) s_{33}; (△) s_{23}; (▽) s_{22}. The error bars are reduced by a factor of two for clarity

symmetric in γ-BHET crystals, and was very nearly so in the α phase[12].

FURTHER ANALYSIS AND DISCUSSION

Shifts for stressed samples

We have previously shown[1] that the shifts for the isotropic and uniaxially oriented samples studied here accord well with certain rather general theoretical predictions concerning their interrelationships. We now attempt to interpret them in a more physical way. We use the notation S^k_{ij} for the shift measured when the incident and scattered beams are polarized in the OX_j and OX_i directions and the stress is applied parallel to OX_k.

The simplest question that can be asked about any of the shifts is whether it depends on the macroscopic stress or the macroscopic strain in the sample. Within the linear elastic region these are linearly related and the question is irrelevant; once creep takes place, however, they are no longer linearly related. The data shown in *Figure 2* for sample C indicate clearly that the shifts vary linearly with the macroscopic applied stress and not so with the strain. This remains true even when the strain increases during creep. The shifts S^3_{33} and S^1_{33} observed for loading sample

Table 5 Changes in intensities (by area) with stress

Intensity	True stress (MPa)	Average strain (%)	Ratio of loaded to unloaded intensity
Sample A ($\lambda = 1$)			
Tensile stress σ_3			
I_{33}	23.57	1.08	1.018 ± 0.003
I_{11}	23.57	1.08	0.980 ± 0.004
I_{21}	23.57	1.08	0.993 ± 0.005
I_{13}	23.57	1.08	1.031 ± 0.005
Sample B ($\lambda = 3.38$)			
Tensile stress σ_3 parallel to draw			
I_{33}	67.81	2.00	1.025 ± 0.006
I_{11}	67.81	2.00	0.989 ± 0.006
I_{21}	67.81	2.00	0.964 ± 0.005
I_{13}	67.81	2.00	1.006 ± 0.007
Tensile stress σ_1 perpendicular to draw			
I_{33}	14.23	0.72	0.983 ± 0.003
I_{11}	14.23	0.72	1.006 ± 0.010
I_{22}	14.23	0.72	0.991 ± 0.009
I_{21}	14.23	0.72	1.005 ± 0.004
I_{13}	14.23	0.72	0.985 ± 0.006
I_{23}	14.23	0.72	0.985 ± 0.005
Sample C ($\lambda = 4.71$)			
Tensile stress σ_3 parallel to draw			
I_{33}	123.68	2.20	1.062 ± 0.026
I_{11}	133.93	2.40	0.957 ± 0.011
I_{21}	133.93	2.40	0.987 ± 0.008
I_{13}	133.93	2.40	1.014 ± 0.006
Tensile stress σ_1 perpendicular to draw			
I_{33}	17.60	1.00	1.068 ± 0.032
I_{11}	16.36	0.92	1.071 ± 0.021
I_{22}	15.70	0.90	0.970 ± 0.009
I_{21}	15.70	0.90	1.012 ± 0.011
I_{13}	15.70	0.90	1.037 ± 0.005
I_{23}	15.70	0.90	0.991 ± 0.005
Sample D ($\lambda = 3.93$)			
Tensile stress σ_3 parallel to draw			
I_{33}	121.59	1.83	1.017 ± 0.005
I_{11}	121.59	1.83	0.958 ± 0.008
I_{21}	121.59	1.83	0.981 ± 0.006
I_{13}	121.59	1.83	0.998 ± 0.003

C parallel to OX_3 and parallel to OX_1, respectively, show that the shift produced by chains close to the draw direction (OX_3) cannot depend simply on the macroscopic stress in that direction. This follows from the fact that the S_{33} shift measures the shift due predominantly to chains oriented close to the draw direction[2], and the shift S_{33}^1 for loading parallel to OX_1 is almost as large as the shift S_{33}^3 for loading parallel to OX_3, although it has the opposite sign; the overall state of stress in the sample is important.

The last observation suggests that the S_{33} shift might be determined by the strain parallel to OX_3, corresponding to the linear region of the stress–strain curve at short times. A simple argument shows that this is not so. The strains parallel to OX_3 are in the ratio of the compliances $s_{33}/s_{31} = -1/\nu_{13}$ for equal stresses parallel to OX_3 and OX_1, and the value of ν_{13} for sample C must be close to 0.43 ± 0.06 (ref. 16), giving $s_{33}/s_{31} = -2.3 \pm 0.3$. The ratio of the shifts S_{33}^3/S_{33}^1 is, however, -1.3 ± 0.2.

The above results suggest that the contribution to the shift produced by a given set of chains may depend on the overall state of resolved stress or short-time strain expressed with respect to that set of chains. For loading parallel to OX_3, chains making the same angle θ to the draw direction will, on average, experience the same stress field irrespective of their azimuthal angle around the draw direction. If the macroscopic stress in the sample is due only to a stress σ parallel to OX_3, the resolved stress parallel to a chain at angle θ to OX_3 is equal to $\sigma \cos^2 \theta$, and the resolved stresses normal to the chain and parallel and perpendicular, respectively, to the plane containing the chain axis and the OX_3 axis are $\sigma \sin^2 \theta$ and 0. If it is assumed that the shift in wavenumber of the vibrational frequency for this chain is linearly related to the resolved stress parallel to the chain axis and the mean resolved stress perpendicular to the chain axis, it follows that the shift observed for the whole sample per unit applied stress will be

$$S_{ij}^3 = a\langle \cos^2 \theta \rangle_{ij} + \frac{1}{2} b \langle \sin^2 \theta \rangle_{ij} \quad (1)$$

where the averages must be weighted not only for the orientation distribution but also for the preferential contribution made to the Raman intensity I_{ij} by chains at different angles θ, and a and b are coefficients characteristic of the vibrational mode studied. A computer program was written to calculate the averages which were then used in a spreadsheet to perform a weighted least-squares fit of the four shifts for the uniaxially loaded sample C to find a and b. In this fit the distribution of orientations was taken to be the most probable distribution for the values $\langle P_2(\cos \theta) \rangle = 0.611$ and $\langle P_4(\cos \theta) \rangle = 0.418$ found from the Raman intensity data. The results of the fit are shown in *Table 6*, together with the values of a and b obtained. The fit is only moderately good, with $\chi^2 = 49.9$ for a two-parameter fit to four data values.

As explained elsewhere[1], it is possible to deduce from the shifts observed with loading parallel to OX_1 a set of shifts that would be observed for uniaxial dilational loading around OX_3, i.e. the shifts that would be observed for a uniform stress in all directions perpendicular to OX_3. We call these shifts S_{ij}^d. The values shown in *Table 6* were obtained by taking the parts of the stress sensitivities shown in *Table 4* which are symmetric with respect to OX_3, and these should be doubled to obtain true stress sensitivities to a uniform dilational stress. These data can be fitted in a similar way to the data for the uniaxial tensile stress, except that the appropriate equations are now of the form

$$S_{ij}^d = \frac{1}{2} a \langle \sin^2 \theta \rangle_{ij} + \frac{1}{4} b \langle 1 + \cos^2 \theta \rangle_{ij} \quad (2)$$

where a and b should have the same values as before. The data in *Table 6* show the corresponding fit, together with the values of a and b required. The fit is good, with $\chi^2 = 0.54$, but the values of a and b determined from this fit are very different from those for the first fit. Also in *Table 6* are the results of an attempt to fit all eight shifts simultaneously. The fit is rather poor, with $\chi^2 = 97.2$ for a two-parameter fit to eight data values.

So far the fits have been made under the assumption of uniform stress within the sample. Similar calculations were carried out assuming uniform strain within the sample and assuming that the shift for a given chain is linearly related to the short-time resolved strain parallel to the chain axis and the mean resolved strain perpendicular to the chain axis. It follows that the

Table 6 Fits of the uniform stress and uniform strain calculations to the experimental stress sensitivities of the shifts for drawn sample C

		Calculated shift sensitivities (cm^{-1} GPa^{-1})					
		Uniform stress			Uniform strain		
Measured sensitivity (cm^{-1} GPa^{-1})	Uncertainty	Tensile fit	Dilational fit	Fit to all eight	Tensile fit	Dilational fit	Fit to all eight
Tension							
−6.05	0.18	−5.28		−5.36	−5.28		−5.34
+0.00	0.52	+0.36		+0.57	+0.36		+0.28
−0.34	0.27	+0.11		+0.30	+0.11		+0.03
−3.08	0.17	−3.98		−4.00	−3.98		−4.05
Dilation							
+4.64	0.55		+4.67	+2.85		+4.67	+3.70
−7.07	1.37		−6.41	−0.12		−6.41	−2.57
−5.05	1.60		−5.91	+0.01		−5.91	−2.28
+2.22	0.83		+2.13	+2.17		+2.13	+2.26
χ^2		49.90	0.54	97.22	49.90	0.54	67.03
a		−6.29	−29.97	−6.42	a' −42.19	−91.41	−46.83
b		6.05	13.32	6.76	b' 27.91	15.48	18.38

shifts observed for the whole sample will be given by

$$S_{ij}^3 = (a'T_1 + \frac{1}{2}b'T_2)s_{33} \quad (3)$$

for tensile strain, where

$$T_1 = \langle\cos^2\theta\rangle_{ij} - \nu_{13}\langle\sin^2\theta\rangle_{ij}$$

$$T_2 = (1 - \nu_{13})\langle\sin^2\theta\rangle - 2\nu_{13}\langle\cos^2\theta\rangle_{ij}$$

and

$$S_{ij}^d = (\frac{1}{2}a'D_1 + \frac{1}{4}b'D_2)s_{11} \quad (4)$$

for dilational strain, where

$$D_1 = (1 - \nu_{21})\langle\sin^2\theta\rangle_{ij} - 2\nu_{31}\langle\cos^2\theta\rangle_{ij}$$

$$D_2 = 2(1 - \nu_{21})\langle\cos^2\theta\rangle_{ij} + (1 - \nu_{21} - 2\nu_{31})\langle\sin^2\theta\rangle_{ij}$$

The measured 10 s compliances were used and the values of the Poisson's ratios ν_{ij} were again taken from reference 16.

The results of these fits are also given in *Table 6*. The fits for tensile and dilational strain are identical to those obtained using the assumption of uniform stress, as they must be; the fit for all eight shifts is slightly better but still rather poor. Further fits were undertaken in which a term was introduced to allow the shifts to depend on either the resolved shear stress or shear strain with respect to a chain. These fits were significantly better for the tensile fits, as expected with an extra parameter, but only marginally better for the fits to all eight shifts, and are therefore not reported in detail. The conclusion must be that it is not possible to explain the observed shifts in terms of such simple models, and we therefore do not report fits for the other samples. In the paper concerned with the necessary interrelationships between the fits[1], the form of the function $f(\theta)$ which describes the average contribution to the shift produced by a chain making angle θ with the stress axis was deduced for a random sample. The form of $f(\theta)$ was found to be somewhere between that expected if the shift were proportional to the tensile component of the macroscopic stress resolved parallel to the chain and that expected if the shift were proportional to the tensile component of the macroscopic strain resolved parallel to the chain. It seems likely that a similar result would be found for uniaxially oriented samples if such a function could be deduced, and this may be the reason for the failure of the simple models proposed here.

Another demonstration of the deficiency of the assumption that the mean shifts due to chains at various orientations depend only on the macroscopic resolved stress or strain with respect to the chains is afforded by calculating the shift sensitivities for a completely isotropic applied stress or strain. For isotropic stress it is only necessary to take the stress sensitivities for the uniaxial tensile stress and add twice the corresponding sensitivities shown in *Table 6* for the dilational stress. For isotropic strain the required combination involves the compliances and Poisson's ratios. The resulting sensitivities for samples A, B and C are given in *Table 7*, where the strain sensitivities are those for a strain equal to that for a random sample subjected to a negative pressure of 1 GPa. If either of the simple assumptions were true, one of these sets of shifts would be independent of the polarization conditions since, on average, the stress or strain on a chain is independent of its orientation when the stress or strain is isotropic. The fact that the different polarization conditions are sensitive to chains in different orientations would then no longer matter. The shifts should also be independent of the sample. Neither set of shifts is independent of polarization conditions or sample, but once again the strain set comes nearer to satisfying the assumptions.

Residual stress in drawn samples

The position of the 1616 cm^{-1} line for the oriented but not loaded sample C was found to be very slightly

different from that for the unoriented sample A and to depend upon the polarization conditions. A possible reason for this could be the existence of built-in residual stress in the chains. Since the original drawing was uniaxial, the distribution of stresses might be expected to be of the same type as that produced on subsequent loading. If this were the case, it should be possible to deduce the residual stress by fitting the 'shifts' between the positions for the drawn and undrawn samples using the stress sensitivities deduced from the loading experiments on the drawn sample. *Table 8* shows the results of least-squares fitting the 'shifts' to the stress sensitivities using a single scaling factor for all four 'shifts'. The fit gives $\chi^2 = 8.39$ and the scaling factor corresponds to a stress of 35 MPa. This is in good agreement with a direct determination of the stress on a sample drawn under exactly the same conditions as sample C, where the final stress during drawing was 44 MPa.

Intensity changes on stressing

When a sample is subjected to stress within the elastic region, there are at least two possible reasons why the intensity of the Raman scattering due to a particular vibrational mode for particular polarization conditions might change. The first is that the strain in the sample implies a new distribution of orientations of the chains, and the intensities are sensitive to orientation. The second is that there may be changes in both the absolute strength of the Raman scattering and the form of the Raman tensor, i.e. the ratios of its components, for a chain under stress. It is assumed that effects due to small changes in refractive index are negligible.

The orientational effect can be estimated by making the assumption that the applied stress causes an affine deformation of the pre-existing distribution of orientations. This is essentially the same as the assumption of uniform strain in the sample. If δP_2 and δP_4 represent the changes in $\langle P_2(\cos\theta)\rangle$ and $\langle P_4(\cos\theta)\rangle$, respectively, it is shown in the Appendix that for uniaxial applied strain parallel to the draw direction this assumption leads to

$$\delta P_2 = 3(1+\nu_{13})e_3(C_2 - C_4) \quad (5)$$

$$\delta P_4 = \frac{5}{2}(1+\nu_{13})e_3(-3C_2 + 10C_4 - 7C_6) \quad (6)$$

where ν_{13} is the Poisson's ratio, e_3 is the longitudinal strain and $C_n = \langle\cos^n\theta\rangle$. It is also shown that for a uniaxial dilational strain the same equations apply except that $(1+\nu_{13})e_3$ is replaced by $-(1+\nu_{31})e_1$.

Since each observed intensity can be written in the form[2,4,17]

$$I_{ij} = [a_{ij} + b_{ij}\langle P_2(\cos\theta)\rangle + c_{ij}\langle P_4(\cos\theta)\rangle]I_0 \quad (7)$$

where I_0 is independent of i and j, it follows that

$$\frac{\delta I_{ij}}{I_{ij}} = \frac{b_{ij}\delta P_2 + c_{ij}\delta P_4}{a_{ij} + b_{ij}\langle P_2(\cos\theta)\rangle + c_{ij}\langle P_4(\cos\theta)\rangle} \quad (8)$$

It then follows that the ratio of the fractional intensity changes observed for uniaxial and dilational strains should be independent of the polarization conditions and should be equal to $-(1+\nu_{31})e_1/(1+\nu_{13})e_3$. The experimental data are not consistent with this. It is, however, interesting to see whether the intensity changes predicted by the affine assumption would contribute significantly to the observed changes. The quantities C_2 and C_4 are easily calculated from $\langle P_2(\cos\theta)\rangle$ and $\langle P_4\cos\theta)\rangle$ and C_6 can be estimated in two ways, either by using the inequality[18]

$$C_4^2/C_2 \le C_6 \le (C_4 - C_4^2 - C_2^2 + C_2C_4)/(1 - C_2) \quad (9)$$

or from the most probable distribution for the given values of $\langle P_2(\cos\theta)\rangle$ and $\langle P_4(\cos\theta)\rangle$. The mean of the two extreme values given by the inequality was used here.

Table 9 shows a comparison of the observed and calculated fractional changes in intensity for uniaxial loading of sample C. For the uniaxial dilation the components of the observed changes that are symmetric with respect to OX_3 are taken. The changes of intensity predicted by the affine assumption are of the same order of magnitude as the observed changes for the uniaxial tensile stress and must therefore be taken into account in any attempt to understand the observed changes in terms of changes of the Raman tensor for chains under stress.

For the uniaxial dilation the predicted changes of

Table 7 Calculated stress sensitivities of shifts for uniform stress or strain

	Stress sensitivities (cm^{-1} GPa^{-1})		
Shift	A ($\lambda = 1$)	B ($\lambda = 3.38$)	C ($\lambda = 4.71$)
Uniform stress			
S_{33}	-6.0 ± 1.5	$+0.4 \pm 2.2$	$+3.2 \pm 1.1$
S_{11}	-6.0 ± 1.5	-8.5 ± 2.5	-14.1 ± 2.8
S_{21}	-8.5 ± 3.4	-9.5 ± 2.5	-10.4 ± 3.2
S_{13}	-8.5 ± 3.4	-4.9 ± 2.9	$+1.4 \pm 1.7$
Uniform strain			
S_{33}	-6.0 ± 1.5	-1.1 ± 1.7	-1.9 ± 0.8
S_{11}	-6.0 ± 1.5	-6.1 ± 2.1	-6.4 ± 1.6
S_{21}	-8.5 ± 3.4	-7.1 ± 2.0	-4.9 ± 1.6
S_{13}	-8.5 ± 3.4	-4.5 ± 2.2	-1.1 ± 0.8

Table 8 Least-squares fits to the stress sensitivities of the 'shifts' between unloaded undrawn sample A and unloaded drawn sample C

Polarization	Sensitivity (cm^{-1} GPa^{-1})	'Shift' (cm^{-1})	Calculated 'shift' (cm^{-1})
33	-6.05 ± 0.18	-0.170 ± 0.036	-0.209
11	$+0.00 \pm 0.52$	-0.067 ± 0.027	$+0.000$
21	-0.34 ± 0.27	-0.053 ± 0.026	-0.012
13	-3.08 ± 0.17	-0.127 ± 0.023	-0.107

Table 9 Fractional changes in intensity for uniaxial tensile and uniaxial dilational stress for sheet C ($\lambda = 4.71$)

	Fractional changes in intensity	
Intensity	Observed	Calculated, affine
Tensile stress $\sigma_3 = 133.93$ MPa		
I_{33}	$+0.067 \pm 0.028$	$+0.012$
I_{11}	-0.043 ± 0.011	-0.026
I_{21}	-0.013 ± 0.008	-0.026
I_{13}	$+0.014 \pm 0.006$	-0.004
Dilational stress $\sigma_1 = \sigma_2 = 8.80$ MPa		
I_{33}	$+0.068 \pm 0.032$	-0.0011
I_{11}	$+0.022 \pm 0.013$	$+0.0024$
I_{21}	$+0.013 \pm 0.012$	$+0.0024$
I_{13}	$+0.016 \pm 0.004$	$+0.0004$

intensity are smaller than the observed changes and are negligible in comparison with the experimental uncertainties. All the observed effects must be due to changes in the nature of the Raman tensor, and this is borne out by a calculation of the orientation independent intensity sums[17], given by $I_{11} + I_{22} + I_{33} + 2I_{12} + 2I_{13} + 2I_{23}$. For the unstressed sample C the value of this quantity (taking $I_{33} = 100$ for the unstressed sample) was 204.4, and for the same sample under the tensile stresses parallel to OX_3 and OX_1 shown in *Table 9* it was 211.6 ± 2.7 and 213.9 ± 3.2, respectively, on the same basis. Both changes are significant, but that for the stress parallel to OX_1 is much larger when account is taken of the fact that this stress was much smaller than the stress parallel to OX_3.

CONCLUSIONS

The results described and discussed above show that it is not possible to explain the frequency shifts observed for the $1616\,cm^{-1}$ Raman line of PET, when samples are stressed in various directions and various polarization conditions are used, in terms of the simple models considered, which assume that the average shifts contributed by chains at various angles to the draw direction are related simply to the state of either macroscopic stress or macroscopic strain expressed in terms of axes fixed in the chains. This suggests that great care should be taken in the interpretation of Raman shifts observed when studying non-uniformly stressed samples in an attempt to deduce the stress distributions within them. It was also found that the intensity changes observed under stress could not be explained in terms of affine changes of molecular orientation alone; there must also be changes in the magnitude and form of the Raman tensor.

ACKNOWLEDGEMENTS

We are grateful to the SERC/EPSRC for providing a research grant which supported E. L. V. L. and to ICI for the provision of PET sheet. We thank Mr S. F. Johnston for making improvements to the Raman system which greatly increased the ease of data collection and processing, and Mr P. L. Carr for preparing sample D.

REFERENCES

1 Bower, D. I., Lewis, E. L. V. and Ward, I. M. *Polymer* 1995, **36**, 3473 and references therein
2 Fina, L. J., Bower, D. I. and Ward, I. M. *Polymer* 1988, **29**, 2146
3 Daubeny, R. de P., Bunn, C. W. and Brown, C. J. *Proc. R. Soc. London, Ser. A* 1954, **226**, 531
4 Jarvis, D. A., Hutchinson, I. J., Bower, D. I. and Ward, I. M. *Polymer* 1980, **21**, 41
5 Gupta, V. B. and Ward, I. M. *J. Macromol Sci., Phys. B* 1967, **1**, 373
6 Hadley, D. W., Pinnock, P. R. and Ward, I. M. *J. Mater. Sci.* 1969, **4**, 152
7 Ladizesky, N. H. and Ward, I. M. *J. Macromol. Sci., Phys. B* 1971, **5**, 661
8 Lewis, E. L. V. and Ward, I. M. *J. Macromol. Sci., Phys. B* 1980, **18**, 1
9 Lewis, E. L. V. *J. Mater. Sci.* 1979, **14**, 2343
10 Everall, N. J. and Lumsdon, J. *Spectrosc. Eur.* 1992, **4**, 10
11 Bower, D. I., Jarvis, D. A. and Ward, I. M. *J. Polym. Sci., Polym. Phys. Edn* 1986, **24**, 1459
12 Lewis, E. L. V. and Bower, D. I. *J. Raman Spectrosc.* 1987, **18**, 61
13 Purvis, J., Bower, D. I. and Ward, I. M. *Polymer* 1973, **14**, 398
14 Huijts, R. A. and Peters, S. M. *Polymer* 1994, **35**, 3119
15 Lewis, E. L. V., Bower, D. I. and McDonald, W. S. *Acta Crystallogr., Sect. C* 1983, **39**, 410
16 Ward, I. M. 'Mechanical Properties of Solid Polymers', 2nd Edn, Wiley, Chichester, 1983, p. 279
17 Bower, D. I. *J. Polym. Sci., Polym. Phys. Edn* 1972, **10**, 2135
18 Bower, D. I. *J. Polym. Sci., Polym. Phys. Edn* 1981, **19**, 93

APPENDIX

Fluorescence

The Raman spectra of many polymers show background 'fluorescence' when the spectra are excited by visible light; PET is no exception. The fluorescence was removed by bathing the sample in the laser beam until the intensity scattered at $1550\,cm^{-1}$ (far from any spectral line) had decreased to a constant value; this took 3–4 h. It was particularly important to remove fluorescence in the present experiments: if the overall background intensity was still decreasing owing to fluorescence during a run, this would alter the line shape and shift the line position appreciably. For each loaded run, the sample was moved up to bring the defluoresced region back into the beam before recording the spectrum.

Polarization scrambling

When the polarized laser beam passes completely through a sample it is possible to detect radiation polarized perpendicular to the original polarization direction, even when this is parallel to a principal axis of the sample. We call this 'polarization scrambling'. Such scrambling causes a mixing of the intensities I_{ij}. If polarization scrambling is present, the following scramblings take place:

1. In SG X_2X_1, I_{33} and I_{23} (Vv and Vh) scramble into each other, and I_{31} and I_{21} (Hv and Hh) do so, too.
2. In SG X_1X_2, I_{33} and I_{32} (Vv and Hv) scramble into each other, and I_{13} and I_{12} (Vh and Hh) do so, too.
3. In SG X_2X_2 there is no scrambling: all of I_{33}, I_{11}, I_{13} and I_{31} are 'clear'.
4. In SG X_1X_1, all of I_{33}, I_{22}, I_{23} and I_{32} will scramble into each other.

It was found by direct measurement that there was negligible scrambling of the laser beam when it passed through the sample parallel to OX_2, probably because the sample is thin in this direction and it is assumed that polarization scrambling of the laser beam does not produce any significant intensity polarized parallel to the original beam propagation direction.

If I_{ij}^m is the measured intensity corresponding to the true intensity I_{ij}, the result of this scrambling is that I_{23}^m and I_{32}^m will have a proportion of I_{ii} (I_{11}, I_{22} or I_{33}) in them, and, since I_{ii} is about twice I_{ik} ($k \neq i$) (the depolarization ratio), they will therefore be too high. On the other hand, I_{12}^m and I_{13}^m along with I_{21}^m and I_{31}^m merely scramble into each other (or not at all in X_2X_2). This helps to explain the intensity distribution shown in *Table 3* for the undrawn sheet A.

In the drawn sheets B, C and D, there is greater transmission in the OX_1 propagation direction and less

Table A1 Transmission and scrambling of the laser beam on passing through samples for different directions of normal incidence on the sample and for different polarization directions (V or H). The solid angle at the detector was 0.0022 sr

	Transmission (%)				Scrambling[b] (%)			
	A	B	C	D	A	B	C	D
OX_3 axis vertical								
OX_1 propagation								
t^a (mm)	6.2	1.38	2.9	0.76	6.2	1.38	2.9	0.76
V (OX_3)	6.6	22.8	17.2	31.5	2.24	0.48	0.54	1.72
H (OX_2)	5.9	23.7	15.8	40.0	2.22	0.43	0.15	0.51
OX_2 propagation								
t^a (mm)	0.184	0.098	0.082	0.127	0.184	0.098	0.082	0.127
V (OX_3)	81.9	54.1	48.6	88.2	0.64	0.02	0.37	0.04
H (OX_1)	82.2	69.7	65.0	86.2	0.28	0.01	0.15	0.27
OX_1 axis vertical								
OX_2 propagation								
t^a (mm)		0.103	0.082			0.103	0.082	
V (OX_1)		77.8	75.8			0.05	0.27	
H (OX_3)		59.3	55.3			0.14	0.24	
OX_3 propagation								
t^a (mm)		1.58	8.1			1.58	8.1	
V (OX_1)		40.7	4.6			0.21	1.12	
H (OX)2)		40.8	4.0			0.33	0.26	

[a] The thickness of the sample in the direction of propagation. The number of significant figures quoted gives an indication of the accuracy to which the corresponding thickness could be measured

[b] The degree of scrambling is the ratio of light power measured with an analyser oriented at right angles to the direction of incident polarization, expressed as a percentage of the power measured in the incident direction of polarization after the beam has passed through the sample

polarization scrambling (*Table A1*) than for the undrawn sheet A. In addition to the above scramblings, in SG $X_3X_3/1$ all of I_{11}, I_{22}, I_{12} and I_{21} will scramble into each other.

A scrambling model was devised in which the intensities, for $p \neq 2$, were of the following form. For the 90° SGs

$$I_{ij}^m = (1 - f_{2p})I_{ij} + f_{2p}I_{kj} \qquad (k \neq i \text{ and } k \neq p) \quad \text{(A1)}$$

for SG X_2X_p and

$$I_{ij}^m = (1 - f_{p2})I_{ij} + f_{p2}I_{ik} \qquad (k \neq j \text{ and } k \neq p) \quad \text{(A2)}$$

for SG X_pX_2. For the 180° SGs $X_1X_1/3$ ($p = 1$) and $X_3X_3/1$ ($p = 3$), for $j \neq i$ and $i, j \neq p$

$$I_{ii}^m = (1 - f_{pp})^2 I_{ii} + f_{pp}^2 I_{jj} + 2f_{pp}(1 - f_{pp})I_{ij} \quad \text{(A3)}$$

for Vv and Hh and

$$I_{ij}^m = [(1 - f_{pp})^2 + f_{pp}^2]I_{ij} + f_{pp}(1 - f_{pp})(I_{ii} + I_{jj}) \quad \text{(A4)}$$

for Vh and Hv.

In these equations, $1 - f$ is the fraction of I_{ij} remaining as I_{ij} after the beam has travelled through the sample, and p takes the value 1 or 3. The values of f for each SG (f_{pq} for SG X_pX_q etc.) were found for the undrawn sheet A by assuming isotropy, taking the depolarization ratio $\rho_l = I_{ik}/I_{ii}$ from the 'clear' SG $X_2X_2/3$, and solving the equations obtained by taking the ratios of the equations for Vh, Hv and Hh to the equation for Vv from equations (A1) or (A2) and from (A3) and (A4), all for $p = 1$. In each case three values for the appropriate f were obtained and averaged. The three average values and the value of ρ_l were then used to predict the ratios of the expected measured intensities. Comparison with the observed ratios showed satisfactory agreement, suggesting that the model was valid for sheet A. For the drawn sheets, the calculations were tried first for C, assuming uniaxial anisotropy. For $p = 1$, equations (A1)–(A4) plus the value of I_{13} from the 'clear' SG $X_2X_2/3$ provide enough equations to solve for the values of I_{ij}. For $p = 3$ there are too many unknown quantities and the equations cannot be solved. The intensities I_{13}, I_{31}, I_{23} and I_{32} calculated for sheet C by this procedure then agreed with each other much better, but I_{22} from SG $X_1X_1/3$ Hh was still too high.

Differential scattering

It was noticed that the light transmission in the drawn sheets B and C, but not in D nor the undrawn A, was significantly less whenever the light was polarized parallel to OX_3 than when the polarization was parallel to OX_1 (*Table A1*). By eye, the samples looked 'milky' whenever incident or scattered light was polarized parallel to the draw direction for a wide range of scattering angles, and this light was scattered into a disc whose normal was parallel to the draw direction. For

light polarized perpendicular to the draw direction, the drawn samples looked much clearer. There was negligible loss of linear polarization of the scattered light after passing through the sample thickness (negligible polarization scrambling).

This meant that whenever the beam passed through the sample polarized parallel to the draw direction, it would be scattered out and therefore effectively reduced in intensity more than when polarized perpendicular to draw: this would then affect the measured intensities. The intensity loss was taken to be of the form

$$I(x) = I_0 \exp(-\mu_i x) \tag{A5}$$

where μ_i is a scattering (effectively an absorption) coefficient per millimetre for the electric vector parallel to i. The μ_i were calculated for sheet C from the measured transmittances and thicknesses of the sample (*Table A1*). The average intensity along the ray is given by integration and is proportional to

$$(\mu_i d)^{-1}[1 - \exp(-\mu_i d)] \tag{A6}$$

where d is the distance travelled in the sample, which depends on the SG, on where the beam is incident on the sample and on the acceptance length of the spectrometer slit. There is a possibility of mixing in other intensities in some polarization combinations via secondary scattering, in which a scattered incident beam is rescattered back at a different angle into the volume of the sample observed by the spectrometer.

The scattering coefficients were found to be $\mu_1 = \mu_2 = 0.84\,\text{mm}^{-1}$ and $\mu_3 = 2.0\,\text{mm}^{-1}$. However, in these thin samples of width-to-thickness ratio ~ 35, whenever the incident beam is along a long direction (OX_1 or OX_3), total internal reflection would 'channel' some of the scattered light into the observable volume instead of it being scattered out of the sample. A simple calculation via Snell's law showed that μ_1 would be effectively reduced to $\sim 0.42\,\text{mm}^{-1}$, and μ_3 to $1.0\,\text{mm}^{-1}$, whenever the incident ray was parallel to OX_1 (there is no differential scattering parallel to OX_3). The results found after correcting the intensities in this way for sample C are shown in *Table 3*. It can be seen that the agreement between I_{11} and I_{22} (especially I_{22} from $X_1X_1/3$ Hh) and between I_{13}, I_{31}, I_{23} and I_{32} is greatly improved, without the need for introducing polarization scrambling and its mixing in of some intensities. Secondary scattering was found to be negligible by inspection of the intensities. Similar calculations were performed for sheet B. No significant scattering was observed for sample D.

Affine deformation

Let θ_0 be the angle between the draw direction and a given chain axis before stress is applied and let θ be the corresponding angle when the stress is applied. Then (see *Figure A1*)

$$\tan\theta = \left(\frac{1 - \nu_{13}e_3}{1 + e_3}\right)\tan\theta_0 \tag{A7}$$

where e_3 is the tensile strain and ν_{13} is the Poisson's ratio. Thus, writing $\cos^n\theta = C^n$

$$\frac{1 - C^2}{C^2} = [1 - 2(1 + \nu_{13}e_3)]\frac{1 - C_0^2}{C_0^2} \tag{A8}$$

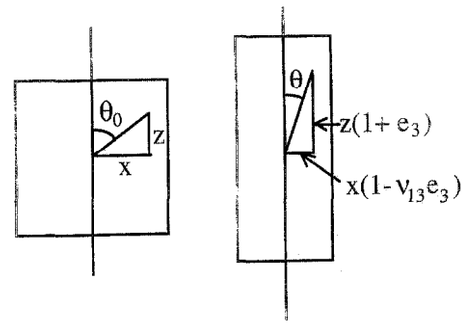

Figure A1 Rotation of a chain segment by affine deformation for uniaxial extension

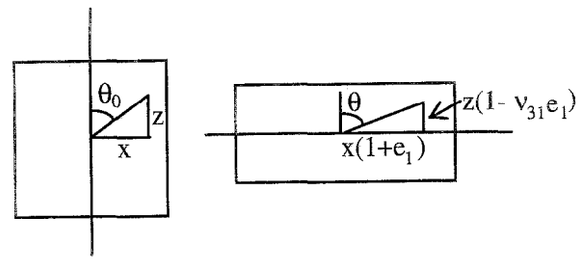

Figure A2 Rotation of a chain segment by affine deformation for uniaxial dilation

where C_0^2 is the value of C^2 for $\theta = \theta_0$. Expanding to first order in e_3, assuming that the changes in C^n are small and dropping the subscript 0 leads to

$$\delta\left(\frac{1 - C^2}{C^2}\right) = -\frac{\delta(C^2)}{C^4} = -2(1 + \nu_{13})e_3\frac{1 - C^2}{C^2} \tag{A9}$$

so that

$$\delta(C^2) = 2(1 + \nu_{13})e_3C^2(1 - C^2) \tag{A10}$$

and

$$\delta P_2 = \frac{3}{2}\delta(C^2) = 3(1 + \nu_{13})e_3(C_2 - C_4) \tag{A11}$$

where $\delta P_2 = \delta\langle P_2(\cos\theta)\rangle$ and $C_n = \langle\cos^n\theta\rangle$.

Using $P_4(\cos\theta) = \frac{1}{8}(3 - 30C^2 + 35C^4)$ leads to

$$\delta[P_4(\cos\theta)] = \frac{5}{4}(7C^2 - 3)\delta(C^2) \tag{A12}$$

Substituting for $\delta(C^2)$ from equation (A10) and taking averages then leads to

$$\delta P_4 = \frac{5}{2}(1 + \nu_{13})e_3(-3C_2 + 10C_4 - 7C_6) \tag{A13}$$

It follows from *Figure A2* that the corresponding results for uniaxial dilational strain are obtained from those above by replacing e_3 by $-\nu_{31}$ and $\nu_{13}e_3$ by $-e_1$, which leads immediately to the result that the changes in δP_2 and δP_4, and hence also the changes in intensity, are given by those for uniaxial tensile strain multiplied by $-(1 + \nu_{31})e_1/[e_3(1 + \nu_{13})]$.